New line intensities for the far infrared bands of the Trans- and Cis-conformer of nitrous acid (HONO), new determination of the Trans-Cis conformer barrier and its impact on the astrophysical detection of nitrous acid in protostellar clouds

W. Tchana Betnga, F. Kwabia Tchana, A. Perrin, L. Manceron, J. Vander Auwera, Francis Hindle, A. Coutens

New line intensities for the far infrared bands of the Trans- and Cis-conformer of nitrous acid (HONO), new determination of the Trans-Cis conformer barrier and its impact on the astrophysical detection of nitrous acid in protostellar clouds

W. Tchana Betnga[a,e], F. Kwabia Tchana[a,*], A. Perrin[b,*], L. Manceron[c,a], J. Vander Auwera[d], F. Hindle[e], A. Coutens[f]

[a] Université Paris Cité and Univ Paris Est Creteil, CNRS, LISA, F-75013 Paris, France

[b] Laboratoire de Météorologie Dynamique/IPSL, UMR CNRS 8539, Ecole Polytechnique, Université Paris-Saclay, RD36, 91128 Palaiseau Cedex, France

[c] Ligne AILES, Synchrotron SOLEIL, L'Orme des Merisiers, St-Aubin BP48, 91192 Gif-sur-Yvette Cedex, France

[d] Spectroscopy, Quantum Chemistry and Atmospheric Remote Sensing (SQUARES), C.P. 160/09, Université Libre de Bruxelles, B-1050 Brussels, Belgium

[e] Laboratoire de Physico-Chimie de l'Atmosphère, Université du Littoral Côte d'Opale, Dunkerque, France

[f] Institut de Recherche en Astrophysique et Planétologie (IRAP), Université de Toulouse, UPS, CNRS, CNES, 9 av. du Colonel Roche, 31028 Toulouse Cedex 4, France

Corresponding authors:

Agnès Perrin : agnes.perrin@lmd.ipsl.fr

Fridolin Kwabia Tchana : fridolin.kwabia@lisa.ipsl.fr

Nb of Tables: 7

Nb of Figures: 10

Keywords: Nitrous acid, Trans-HONO, Cis-HONO, Far-infrared, Line intensities, Trans-Cis conformer barrier, Line list, Astrophysics application

Abstract

The first goal of this work is to improve the determination of the energy difference ($\Delta E_{Cis\text{-}Trans}$) between the ground vibrational state of the Cis- and Trans-HONO conformers of nitrous acid. For this, high resolution spectra were recorded in the 50-200 cm^{-1} spectral region at three different temperatures, 240, 270 and 296 K. The relative line intensities for the B-type transitions of pure rotational bands of Trans-HONO and Cis-HONO achieved from our measurements were combined in least squares fit computations to those measured previously by Sironneau *et al*. [*Sironneau V, Flaud JM, Orphal J, Kleiner I, Chelin P. Absolute line intensities of HONO and DONO in the far-infrared and re-determination of the Energy Difference between the trans- and cis-species of nitrous acid. J Mol Spectrosc 2010;259:100-104*]. In this way, we can significantly improve the accuracy on the HONO conformer energy difference, with a value for $\Delta E_{Cis\text{-}Trans} = 95.8 \pm 9.2$ cm^{-1} compared to $^{SIR}\Delta E_{Cis\text{-}Trans} = 99 \pm 25$ cm^{-1} in the previous study of Sironneau *et al*. The second goal is to generate a line list with "absolute" line intensities for the pure rotational bands in the far infrared region of Trans-HONO and Cis-HONO, with both A- and B-type transitions. This new line list proved to be more faithful for an improved detection of HONO in Astrophysical objects [*Coutens A, Ligterink NFW, Loison JC, Wakelam V, Calcutt H, Drozdovskaya MN, Jørgensen JK, Müller HSP, Van Dishoeck EF, Wampfler SF. The ALMA-PILS survey: First detection of nitrous acid (HONO) in the interstellar medium. Astronomy & Astrophysics 2019;623:L13*].

I. Introduction

Nitrous acid (HONO) has been known for a long time as an important player in the chemistry of the troposphere. This species, which accumulates at night [1], quickly dissociates by subsequent photolysis at sunrise. The photolysis of HONO is a direct source of hydroxyl radical, OH, which is a key species in the photochemical cycles responsible for tropospheric ozone formation, leading to the so called ‘‘photochemical smog’’ in polluted area [2, 3].

In addition, nitrous acid molecule proved recently to be of astrophysical interest. Indeed, since several rotational lines of the Trans-HONO and Cis-HONO conformers were identified in the 92 – 363 GHz spectral region towards component B of the low-mass protostellar binary IRAS 16293–2422 with the Atacama Large Millimeter/Submillimeter Array [4]. For this detection, the authors used the line list quoted for HONO on the JPL catalog [5].

Nitrous acid possesses several infrared signatures that are of possible use for optical detection in the Earth atmosphere. The Infrared Atmospheric Sounding Interferometer (IASI) instrument on the METOP satellite [6] could detect HONO in the 11 µm region during the (rather) exceptional conditions of the large Australian bush fires of February 2009 [7] and of 2019-2020 [8, 9].

In addition, the 7.3 µm region, which corresponds to the ν_3 band of Trans-HONO centered at 1263.207 cm^{-1} [10], proved to be also of potential use for the HONO detection in IASI spectra [11].

To help future detections of HONO at 11 µm by IASI, or by the future Infrared Atmospheric Sounding Interferometer New Generation (IASI-NG; https://iasi-ng.cnes.fr/fr) satellite instrument, we have generated, in Ref. [12], a preliminary version of a spectroscopic line list that involve the ν_4 bands of the Trans-HONO and Cis-HONO, centered at 790.117 cm^{-1} and 851.943 cm^{-1}, respectively. This list, covering the 11 µm region, was generated using the existing spectroscopic parameters at the time, and will need to be improved, mainly in terms of absolute line intensities.

One of the problems that we have to face lies in the fact that, in laboratory conditions, nitrous acid exists only in the form of an equilibrium mixture with other species like NO, NO_2 and H_2O, together with smaller quantities of N_2O_4, N_2O_3, and HNO_3 [13]. As discussed in Ref. [13], it is thus difficult to obtain absolute line intensities for a rovibrational band of nitrous acid. Getting these quantities from a laboratory spectrum requests a good knowledge of the partial pressure of HONO present in the absorption cell during the recording, which is complicated, considering its chemical instability. On the other hand, we can alleviate this problem using a

method that is described later in the text and using the far infrared region, which corresponds to the pure rotational bands of HONO.

The second difficulty is that nitrous acid exists in two conformer forms, Trans-HONO and Cis-HONO, with the vibrational ground state levels of Cis-form located in energy at a difference $\Delta E_{Cis\text{-}Trans}$ above those from the Trans-form. Estimates of the $\Delta E_{Cis\text{-}Trans}$ value in the literature span the range from 99 and 225 cm^{-1} for experimental studies [14-18], or from 97 to 385 cm^{-1} in *ab initio* computations [19-23]. The poor knowledge of the $\Delta E_{Cis\text{-}Trans}$ value affects significantly the quality of the linelist that we have generated for the 11 µm region. Indeed, assuming a local thermodynamic equilibrium (LTE) conditions, the relative concentration of Cis-HONO versus Trans-HONO is governed by the Boltzmann factor in $\exp(\Delta E_{Cis\text{-}Trans}/kT)$. It occurs that, at 11 µm region, the Q-branch structures corresponding to the ν_4 bands of the Trans-HONO and Cis-HONO conformers have almost equal intensity at 296 K. Therefore, at lower temperatures, the absorption maximum corresponding to the Cis-HONO conformer is predicted to decrease significantly in intensity relative to its Trans- counterpart. For example, at 220 K, the Cis-/Trans- peak intensity ratio would vary from ~0.82 with $\Delta E_{Cis\text{-}Trans}$ = 107 cm^{-1} [18] to ~0.69 with $\Delta E_{Cis\text{-}Trans}$= 225 cm^{-1} [17], for the most extreme experimental literature values of the Cis- to Trans-energy difference. A detailed literature review of the experimental and theoretical determinations of $\Delta E_{Cis\text{-}Trans}$ is provided by Sironneau *et al*. [18], and the summary of this inter-comparison of the $\Delta E_{Cis\text{-}Trans}$ values is presented in Table 3 of Ref. [18].

Several experimental determinations used low resolution infrared spectra [14, 15] or oscillator strengths of broad nπ* transitions in the near UV spectra [17]. Concerning resolved line measurements at high resolution, $\Delta E_{Cis\text{-}Trans}$ was first determined by Varna and Curl [16] using microwave techniques. Later on, a new determination was performed by Sironneau *et al*. [18], using this time relative line intensities measured using high resolution Fourier transform spectra recorded at 296 K for the main (HONO) and for its deuterated species (DONO) in the 40-140 cm^{-1} spectral region [24]. In this last paper, the value obtained from DONO had to be corrected to account for the differences between the zero point energies of HONO and DONO. In this way the following values were obtained [18]:

$$^{HONO}\Delta E_{Cis\text{-}Trans} = 99 \pm 25 \text{ cm}^{-1} \text{ (HONO only)}, \qquad \text{Eq. (1)}$$

and

$$^{HONO\text{-}DONO}\Delta E_{Cis\text{-}Trans} = 107 \pm 26 \text{ cm}^{-1} \text{ (averaged for HONO and DONO)} \qquad \text{Eq. (2)}$$

Concerning *ab initio* calculations of this quantity [19-23], at the exception of the calculated value given by Richter *et al*. [23], these predictions are rather far from the experimental values obtained at high resolution [16, 18].

Outlook:

The first goal of the present work, based on new measurements in the far-infrared region, is to prepare, upstream, improvements in the 11 μm line list by improving the accuracy on the $\Delta E_{Cis\text{-}Trans}$ value.

The second goal of this study is to generate a reliable line-list (positions, intensities, lower state energies, partition function, and Einstein coefficients) for the pure rotational bands of nitrous acid, which can be used for future atmospheric or astrophysical purposes. For this use, this list must consider together Trans-HONO and Cis-HONO conformers and must account more precisely for the temperature dependence of the Cis- to Trans- relative concentration.

For these pure rotational bands, the computations of line positions are not a problem, thanks to the work of Dehayem *et al*. [24], while the computation of intensities is more problematic. Also, for pure rotational bands, contrary to rovibrational bands, it is, in principle, possible to compute theoretically "absolute line intensities" from experimental data. For this, several conditions must be fulfilled. First, one must have at our disposal the total partition function for the set of both conformers, and this computation requests the most precise possible knowledge of $\Delta E_{Cis\text{-}Trans}$. Second, these intensities involve the squares of matrix elements of the transition moment operators of the pure rotational bands of Trans-HONO and Cis-HONO on the wavefunctions. The expansions of these dipole moment operators involve, at their zeroth order, the Trans-HONO and Cis-HONO permanent dipole moments, $^{Trans}\mu_0$ and $^{Cis}\mu_0$, respectively, that are already well known from Stark measurements [25]. However, it is also necessary to know the centrifugal distortion correction terms, associated to $^{Trans}\mu_0$ and $^{Cis}\mu_0$, in the expansion of the transition moment operators.

This will be done through the exploitation of high resolution Fourier transform spectra recorded at SOLEIL in the 50 – 200 cm^{-1} spectral region and at different temperatures (240, 270 and 296 K). The relative intensities that we obtained during our investigation were combined with those deduced for HONO during the investigation performed by Sironneau *et al*. [18] to get a new and more accurate value of $\Delta E_{Cis\text{-}Trans}$ for HONO.

In the present work, we consider only the HONO (main) isotopic species, and not DONO for which we do not have any new experimental data, and restrict to HONO (only) the discussion of the literature results.

II. Experimental details

Absorption spectra of HONO at three different temperatures (240, 270 and 296 K) were recorded using the Bruker IFS125HR spectrometer in the far-infrared region (50 to 200 cm^{-1}) at Synchrotron SOLEIL (Saint-Aubin, France) on the AILES Beamline [26]. As HONO is adsorbed and reacts on metal or oxidizable surfaces [27], a special long path gas cell made of glass for the cell cylindrical body, Teflon™ bellows for valve and mirror steering or PTFE-coated aluminum alloy for the flanges [28] was used. The cell was fitted with wedged diamond windows (Advanced Diamond Materials, USA) mounted with Teflon™-coated silicone or Kalrez gaskets (Eriks, France). The cell uses a simple White-type optical multi-pass configuration with gold coated mirrors having a special Al_2O_3 solid protective layer (OPTIMASK, France). A triple-envelope glass cell body has been manufactured (Verrerie Soufflée Normalisée, France) with an inner volume of about 14 liters (15 cm inner diameter × 80 cm length) surrounded by an annular cylindrical space for circulating a cooling ethanol bath and a third envelope for the insulating vacuum (5×10^{-5} mbar). The metal flanges supporting the windows, mirror mounts and viewports were covered with a thick PTFE coating (STIM, France) and the mirrors were mounted on Teflon™ bellows (Elkinger, Germany) allowing for travel and tilt adjustments. The optical path can be adjusted between 2.8 and 42 m and the cell can be cooled to 210 K.

The Bruker IFS125HR interferometer was using synchrotron radiation [29] as the light source (500 mA ring current in 416 equal electron bunches). It was equipped with a Mylar/Si composite beamsplitter and a 4 K dual-band mid IR and FIR detector built in 2021 on the AILES Beamline, using a special HgCdTe photoconductor and a bolometer to probe simultaneously the synchrotron radiation. The detector will be described in a separate publication [30], but a few important details are given here. After sets of apertures with decreasing diameters in 77 K and 40 K radiation shields, the output of the interferometer is focused on a 2.5 mm aperture cooled to 4 K. Next the FIR (< 600 cm^{-1}) and mid IR parts of the modulated IR beam are split by a dichroic metal mesh filter (QMC, Cardiff, UK) before being refocused with 4 K-cooled optics on either a supraconducting Nb bolometer (QMC) for the Far IR part or a HgCdTe photoconductor (Hamamatsu, Japan) with a 1.2mm diameter iris for the mid-IR part as in Ref.

[31]. This detector performs well above 80 cm^{-1}, where the HONO lines contribute for more than 70% of the strongest intensities. Interferograms were acquired (without apodization) at 80 kHz scanner fringe frequency and a maximum optical path difference (MOPD) of 642.857 cm. According to the Bruker definition (resolution = 0.9/MOPD), this corresponds to a resolution of 0.0014 cm^{-1}.

The following procedure was used for the measurements. A background spectrum was first recorded at a resolution of 0.02 cm^{-1} while the cell was being continuously evacuated. Then, HONO was directly synthesized in the absorption cell by mixing measured amounts of NO, NO_2, and gaseous H_2O, this is the same procedure as in Ref. [13]. NO_2, H_2O and NO were successively introduced into the cell with a composition of the mixtures covered the following ranges: 25–32% NO_2, 18–32% H_2O, 43–49% NO. The reaction evolved spontaneously towards the formation of HONO and, after about 1h, the equilibrium was reached and the reaction stopped evolving, reaching proportions of 1–2.5% of HONO, depending on the cell temperature. Finally, spectra were recorded for five different HONO equilibrium mixtures. The five pressures chosen and the number of interferograms recorded and averaged to yield the corresponding spectra are listed in **Table 1**. The estimated partial pressures of HONO are also given in **Table 1**. All the sample spectra were ratioed against the empty cell background spectrum. The root mean square (RMS) signal-to-noise ratio (S/N) in the ratioed spectra ranged between 40 and 100. For the Fourier transformation, a Mertz-phase correction with a 0.5 cm^{-1} phase resolution, a zero-filling factor of 2 and no apodization (boxcar option) were applied to the averaged interferograms. To improve the measurement of line positions, a post zero-filling factor of 4 was applied to the averaged spectrum.

The spectra were calibrated by matching the measured positions of about 40 lines of H_2O observed to reference wavenumbers available in HITRAN [32] with a root mean square (RMS) deviation of 0.00009 cm^{-1}. The absolute accuracy of the measured HONO line positions was estimated as the square root of the sum of squares of the accuracy of the reference H_2O line positions in HITRAN (better than 0.0001 cm^{-1}) plus twice the RMS deviation between the observed frequencies and values listed in HITRAN for H_2O, yielding in total 0.0002 cm^{-1}. **Fig. 1** shows a portion of the spectra observed in this work with highly improved experimental conditions: (i) the use of synchrotron radiation which resulted in a better signal-to-noise ratio; (ii) a resolution twice better; (iii) three different temperatures (240, 270 and 296 K) with larger optical path length, allowing low total pressures in the samples. **Fig. 2** shows the region between 85 and 88 cm^{-1} observed in this work and a comparison with that observed by Sironneau *et al*.

[18]. As can be seen, the new experimental conditions allow a fully resolved spectrum and thus a more accurate analysis.

III. Retrieval of line intensities and uncertainty analysis

3.1. *Retrieval of line intensities*

The line intensities were measured using a multi-spectrum fitting program developed in Brussels [33, 34]. This program adjusts spectroscopic (e.g. line positions, intensities and widths) and spectrum-specific (e.g. baseline) parameters to best-fit synthetic spectra to the observed spectra using a Levenberg-Marquardt non-linear least squares fitting procedure. Each synthetic spectrum is calculated as the convolution of the molecular transmission spectrum with an instrument line shape function, which includes the effects of the finite maximum optical path difference and of the finite source aperture diameter of the interferometer. In the present work, no deviation from this model instrument line shape was observed using the nominal aperture diameter of 2.5 mm. The molecular transmission spectrum was generated on a wavenumber grid characterized by a point spacing 4 times smaller than in the corresponding observed spectrum. After convolution with the instrument line shape function, only the calculated spectral points corresponding to observed spectral points were retained. The background in each spectrum was represented by a polynomial expansion up to the second order (a constant or an affine function was however found sufficient in most cases), and the profile of the lines was modeled using a Voigt function [35] with Gaussian width always held fixed to the value calculated for the Doppler broadening. The measurements were carried out on spectrally restricted intervals, ranging from 0.07 to 0.3 cm^{-1} and containing either a single or several lines. The fitted line parameters were the positions, intensities, and buffer-broadening coefficients. In the equilibrium mixture of HONO, the buffer gas molecules are NO, NO_2 and H_2O. For a line belonging to the active molecule (HONO), the pressure induced broadening is therefore calculated according to

$$\gamma_L = [b_L^0(\text{self})\, x + b_L^0(\text{buffer})\,(1-x)]P_{tot} \qquad \text{Eq. (3)}$$

where x is the mixing ratio of the active molecule and P_{tot} is the total pressure. The self-broadening and self-shift coefficients of all the lines were set to 0.1 and 0.0 $cm^{-1}.atm^{-1}$, respectively. The buffer-broadening coefficient of all the lines was initially set to 0.185 $cm^{-1}.atm^{-1}$. The required initial values of the positions and intensities of pure rotational lines considered in the present work were generated using ground-state rotational constants and transition dipole moment constants of *trans*- and *cis*-HONO from previous studies [18, 24]. The

partial pressure of HONO was estimated from equilibrium constants published in literature [13 and related references], then adjusted to match the experimental spectrum. The value obtained was held constant to fit the integrated absorption cross section of the line. Intensity measurements were made for five spectra at different HONO equilibrium mixtures at three different temperatures (see **Table 1**). A multi-spectrum fitting program was used for the spectra recorded at 296 K and the mono-spectrum option of the program for the spectra recorded at 240 and 270 K. Indeed, for the determination of the energy barrier between the *trans*- and *cis*-HONO ground states, data at different temperatures are required. **Figure 3** presents an example of the results of a fit for the spectrum S3 recorded at 270 K. It contains three lines observed in the spectral range 103.19 to 103.26 cm^{-1} and a total of ten fitted parameters. The absence of the molecular signatures in the residuals suggests that the Voigt profile is adequate to fit the observed lines at this level. **Figure 4** also shows good residuals for the spectra recorded at 240 and 296 K. Finally, in this work, 388 individual lines for *trans*-HONO and 185 for *cis*-HONO were carefully measured. **Table 2** summarizes the number of lines selected for the intensity fits and the range covered in J and K_a. Lines with low quantum number do not appear since they are not observed in the useful spectral range covered here (80–130 cm^{-1}).

3.2. *Uncertainty analysis*

Examination of the fit residuals shows that they are generally less than 5%. However, to estimate the accuracy of the measured intensities also requires considering the uncertainties on the physical parameters, contributions from possible systematic errors [36] as well as the uncertainties derived from the fits, taken as the standard deviation. The various sources of error considered in the present work and their associated uncertainties expressed relative to the line intensities are given in **Fig. 5** for three strong, medium and weak selected lines, representative of the 573 measured lines, i.e. ^{R}Q (19,16), ^{R}Q (32,14) and ^{R}Q (30,16). **Figure 5** shows that pressure, systematic errors and the standard deviations of the fits are the main sources of error. The dominant contributions to the systematic errors arise from shifts in the location of the full-scale (100%) photometric level or measurement noise. The effect of noise and small baseline offsets in these were also taken into account. The 0% level could be checked readily and the 100% level fitted on the spectra in regions without absorptions. In the end, for systematic errors, an arbitrary, but conservative estimate of 2% of the line intensities has been retained here. For each transition, we then calculated an upper limit for the overall uncertainty based on the maximum uncertainty of the individual experimental parameters, i.e. ε_{si} (sample purity), ε_t

(temperature), ε_p (pressure), ε_{pl} (pathlength), ε_{fit} (standard deviation from fit) and ε_{sys} (systematic errors), assuming that these uncertainties are uncorrelated:

$$\varepsilon = \sqrt{\varepsilon_{si}^2 + \varepsilon_t^2 + \varepsilon_p^2 + \varepsilon_{pl}^2 + \varepsilon_{fit}^2 + \varepsilon_{sys}^2} \qquad \text{Eq. (4)}$$

Using Eq. (4) and the experimental relative uncertainties involved, the estimated overall uncertainty (estimated accuracy) for each of the 573 relative line intensities measured was calculated. On average, the estimated accuracy for line intensities is equal to 6.5%.

IV. Analysis for HONO

During the whole analysis, the energy levels of the ground states of Trans-HONO and Cis-HONO were computed using a Watson's A-type Hamiltonian written in the I^r representation, and for this, we used the rotational and centrifugal distortion constants[1] achieved by Dehayem *et al*. [24] for the ground vibrational states of Trans-HONO et Cis-HONO.

4.1. *Definitions*

- For the Trans-HONO conformer form, the intensity of a given line of $H^{16}O^{14}N^{16}O$ in a "natural sample" of nitrous acid is given (in cm^{-1}/(molecule. cm^{-2}) by:

$$^{Trans}k_{\tilde{\nu}}^{N}(T) = a_{iso}\frac{8\pi^3\tilde{\nu}}{4\pi\varepsilon_0 3\,c^{Tot}Z(T)}g_{nucl}\left(1-exp\left(-\frac{c\tilde{\nu}}{kT}\right)\right)exp\left(-\frac{cE_A}{kT}\right)R_A^B \qquad \text{Eq. (5)}$$

while, for the Cis- conformer form, we used a slightly different expression:

$$^{Cis}k_{\tilde{\nu}}^{N}(T) = a_{iso}exp\left(-\frac{c\Delta E_{Cis-Trans}}{kT}\right)\frac{8\pi^3\tilde{\nu}}{4\pi\varepsilon_0 3\,c^{Tot}Z(T)}g_{nucl}\left(1-exp\left(-\frac{c\tilde{\nu}}{kT}\right)\right)exp\left(-\frac{cE_A}{kT}\right)R_A^B \qquad \text{Eq. (6)}$$

Indeed, for the Cis-conformer, Eq. (6) includes the " $\exp\left(-\frac{hc\Delta E_{Cis-Trans}}{kT}\right)$ " term to account for the definition of the J = 0 level of the Cis-conformer relative to the Trans-one.

In these expressions, the letters "A" and "B" and $^{Trans}E_A(J, K_a, K_c)$ and $^{Trans}E_B(J, K_a, K_c)$ (respectively, $^{Cis}E_A(J, K_a, K_c)$ and $^{Cis}E_B(J, K_a, K_c)$) are the upper and lower computed wavefunctions and energy levels relatively to the J=0 energy level for Trans-HONO

[1] As mentioned in Ref. [18], we noted a typing error in Table 2 of Ref. [24] for Cis-HONO, and we used $H_{KJ} = -0.678 \times 10^{-9}$ cm^{-1}, instead of $H_{KJ} = -0.0678 \times 10^{-9}$ cm^{-1}.

(respectively, for Cis-HONO) using the parameters quoted in Table 1 for Trans-HONO, (respectively in Table 2 for Cis-HONO) of Ref. [24].

Indeed, accordingly, the definition of the lower level and upper level of the transition, E_L and E_U respectively, differ for Trans-HONO and Cis-HONO, since one has:

$$^{Trans}E_L = {}^{Trans}E_A(J, K_a, K_c) \text{ and } {}^{Trans}E_U = {}^{Trans}E_B(J, K_a, K_c) \quad \text{Eq. (7)}$$

and

$$^{Cis}E_L = {}^{Cis}E_A(J, K_a, K_c) + \Delta E_{Cis\text{-}Trans} \text{ and } {}^{Cis}E_U = {}^{Cis}E_B(J, K_a, K_c) + \Delta E_{Cis\text{-}Trans} \quad \text{Eq. (8)}$$

In addition,

- $\tilde{\nu}$ is the wavenumber in cm^{-1}, and one has:

$$\tilde{\nu} = (E_B\text{-}E_A) = (E_L\text{-}E_U) \quad \text{Eq. (9)}$$

- a_{iso} = 0.9937 is the isotopic abundance of $H^{16}O^{14}N^{16}O$ in a "natural sample" of nitrous acid.
- g_{nucl} is the nuclear spin factor, which is set to a constant value (g_{nucl} = 1) for all rotational levels of the Cis- and Trans-HONO and will be omitted in the rest of the discussion.
- $^{Tot}Z(T)$ is the "total" partition function of HONO at the temperature T, which includes a contribution from the Trans- and Cis-conformers, $^{Trans}Z(T)$ and $^{Cis}Z(T)$, respectively.

$$^{Tot}Z(T) = {}^{Trans}Z(T) + {}^{Cis}Z(T) \times {}^{Cis\text{-}Trans}Z(T) \quad \text{Eq. (10)}$$

In this latter expression, the term $^{Cis\text{-}Trans}Z(T)$ with

$$^{Cis\text{-}Trans}Z(T) = \exp\left(-\frac{hc\Delta E_{Cis-Trans}}{kT}\right) \quad \text{Eq. (11)}$$

accounts for the population ratio of the rotational levels of Cis-HONO relative to those of Trans-HONO, because of the convention adopted for the J = 0 level of Cis-HONO.

In addition, $^{Trans}Z(T)$ and $^{Cis}Z(T)$ in Eq. (10) are the "classical" vibration-rotation contributions of Trans-HONO and Cis-HONO that are computed as usual [37] in the Harmonic Oscillator Approximation (HOA) as the product of its vibrational and rotational contributions, i.e. for the Trans-form and Cis-form, as:

$$^{Trans}Z(T) = {}^{Trans}Z_{Vib}(T) \times {}^{Trans}Z_{Rot}(T)$$

and

$$^{Cis}Z(T) = {}^{Cis}Z_{Vib}(T) \times {}^{Cis}Z_{Rot}(T) \quad \text{Eqs. (12)}$$

The $^{Trans}Z_{Vib}(T)$ and $^{Cis}Z_{Vib}(T)$ individual vibrational contributions were computed using the usual expressions, with for example for the Trans-form:

$$^{Trans}Z_{Vib}(T) = \prod_{i=1-6}(1-\exp(hc\omega_i / kT))^{-1} \qquad \text{Eq. (13)}$$

where, the i-product is performed on the six (non-degenerate) vibrational fundamental modes of the Trans- [10] or Cis-conformer [38], that are collected for example in Table 4 of Ref. [18]. As for $^{Trans}Z_{Rot}(T)$ and $^{Cis}Z_{Rot}(T)$ they are computed using the usual expression:

$$^{Trans}Z_{Rot}(T) = \sum_{all\,rotational\,levels}(2J+1)\exp\left(-hc\,^{Trans}E_A(J,K_a,K_c)/kT\right). \qquad \text{Eq. (14)}$$

In Eq. (14), the summation in the right hand part of this equation involves the (2J+1) usual factor, where J is the total rotational quantum number.

- In Eq. (5) (resp. Eq. (6)), the Trans- (resp. Cis-) R_A^B factors, are the square of the matrix element of the transformed transition moment operator $\mu_Z^{'}$ for the Trans-conformer (resp. Cis-conformer). For the Trans-conformer form, one can write:

$$R_L^U = \left|\langle 0, J'K_a'K_c'|^{Trans}\mu_Z'|0, J''\ K_a''K_c''\rangle\right|^2, \qquad \text{Eq. (15)}$$

where |0> are the upper and lower vibrational state of the transition, and $^{Trans}\mu_Z'$ is the Z-component of the transformed transition moment operator for the Trans-conformer form [39]. A similar expression can be written for Cis-HONO.

Both the Trans-HONO and Cis-HONO are planar C_s-type molecules, and following symmetry considerations, both A- and B-type rotational transitions are to be observed for the far infrared bands with (ΔK_a = 0, ΔK_c = ±1) and (ΔK_a = ±1, ΔK_c = ±1) selection rules, respectively, on the K_a and K_c rotational quantum numbers.

The expansions of the $^{Trans}\mu_Z'$ and $^{Cis}\mu_Z'$ dipole moment operators include, at its zero[th] order, the permanent dipole moment $^{Trans}\mu_0$, and $^{Cis}\mu_0$, with A- and B-components that are well known from Stark measurements [25]: These results are in debye (1 D = 3.33564 ×10^{-30} C m)

$$^{Trans}\mu_0^A = 1.3829(72)\text{ D and }{}^{Trans}\mu_0^B = 1.3468(170)\text{ D for Trans-HONO}^{\,2} \qquad \text{Eq. (16)}$$

and

$$^{Cis}\mu_0^A = 0.3071(39)\text{ D, }{}^{Cis}\mu_0^B = 1.3943(60)\text{ D for Cis-HONO} \qquad \text{Eq. (17)}$$

[2] These results are in debye (1 D = 3.33564 ×10^{-30} C m)

Due to the values of its rotational constants [24], the rather strong (for Trans-HONO) and rather weak (for Cis-HONO) A-type rotational transitions are predicted to be observable only in the very far infrared region (~20 to 40 cm^{-1}), and therefore, out of the spectral range covered by the FTS spectra recorded here or by Sironneau *et al*. [18].

On the other hand, for both conformers, the B-type components are observable in a rather large spectral range of the far infrared region (50 to 350 cm^{-1}). This type of transition can therefore be used for comparison of line intensities to determine the value of $\Delta E_{Cis\text{-}Trans}$. The computation of intensities for pure rotational transitions involves at its zero order term, the permanent dipole moments of Trans-HONO and Cis-HONO [25]. However, when considering the B-type transitions, it proved, as demonstrated in Ref. [18], that higher order distortion terms have a non-negligible contribution in the expansion of ${}^{Trans}\mu_Z'$ and ${}^{Cis}\mu_Z'$.

More precisely, one has, for these B-type components[3]:

$$ {}^{Trans}\mu_B' = {}^{Trans}\mu_0^B \times \varphi_x + {}^{Trans}\mu_4^B \times \{i\varphi_y, J_z\} + {}^{Trans}\mu_6^B \times \{i\varphi_z, iJ_y\} \quad \text{Eq. (18)} $$

$$ {}^{Cis}\mu_B' = {}^{Cis}\mu_0^B \times \varphi_x + {}^{Cis}\mu_4^B \times \{i\varphi_y, J_z\} + {}^{Cis}\mu_6^B \times \{i\varphi_z, iJ_y\} \quad \text{Eq. (19)} $$

4.2. *Method used for the analyses of the experimental absorptions*

The set of three (relative) experimental integrated absorption coefficients (in cm^{-2}) obtained during this work, here labeled as ^{Trans}Abs(T) and ^{Cis}Abs(T), with T = 240, 270 and 296 K, respectively, concern the 83 – 130 cm^{-1} spectral region. In order to complete this information, we combined these data with those achieved previously in the 43 to 121 cm^{-1} spectral range by Sironneau *et al*. [18]. Indeed, the latter relative intensities, identified in the text as ^{Trans}Abs'(296 K) and ^{Cis}Abs'(296 K), provide complementary information for lines involving medium K_a values.

It is important to emphasize that the four data sets were introduced in a common least squares fit, combining both Trans- and Cis- transitions.

Each of these relative intensities is written as:

$$ {}^{Trans}\text{Abs(T)} = \text{Quant(T)} \times {}^{Trans}k_{\tilde{\nu}}^N(T) \quad \text{Eq. (20)} $$

$$ {}^{Cis}\text{Abs(T)} = \text{Quant(T)} \times {}^{Cis}k_{\tilde{\nu}}^N(T) \quad \text{Eq. (21)} $$

---

[3] When line intensity measurements for A-type rotational transitions become available, it is likely that similar higher order centrifugal corrections will have to be taken into consideration in the expansion of ${}^{Trans}\mu_A'$ and ${}^{Cis}\mu_A'$.

For the present data (T = 240, 270 and 296 K), and, for Sironneau's data:

$$^{\text{Trans}}\text{Abs'}(296\text{ K}) = \text{Quant'}(296\text{ K}) \times {}^{Trans}k_{\tilde{\nu}}^{N}(296\ K) \qquad \text{Eq. (22)}$$

$$^{\text{Cis}}\text{Abs'}(296\text{ K}) = \text{Quant'}(296\text{ K}) \times {}^{Cis}k_{\tilde{\nu}}^{N}(296\ K) \qquad \text{Eq. (23)}$$

In these expressions, the four quantities, Quant(240 K), Quant(270 K), Quant(296 K), and Quant'(296 K) are associated to the four sets of experimental data deduced from the FTS spectra recorded during this work at T = 240, 270 and 296 K, respectively, and during Sironneau's study [18]. These "quantities" (in molecule.cm^{-3}) represent the number of molecules per unit volume and were performed for each experimentally measured line. Therefore, during the (common) least squares fit computation on the four sets of relative intensities, the four "quantities" (Quant(T) and Quant'(296 K)) were refined, together with the truly "physically meaningful parameters" that are :

- The $\Delta E_{\text{Cis-Trans}}$ difference of energies that is involved both in the first line of Eq. (6) for computation of the intensities of Cis-HONO and in the computation of $Z_{\text{Tot}}(T)$ (see Eq. (10-11).
- When it proved to be possible, the centrifugal distortion terms, ${}^{Trans}\mu_4^B$, ${}^{Trans}\mu_5^B$, ${}^{Cis}\mu_4^B$, and ${}^{Cis}\mu_5^B$ appearing in the expansion of ${}^{Trans}\mu_B'$ and ${}^{Cis}\mu_B'$ (see Eqs. (18) and (19)).

The information on the partial pressure of HONO present in the cell during the recording of the spectra that are quoted in **Table 1** could be determined only at the very end of this study.

4.3. *Results of the least squares calculation*

Only three "physically meaningful parameters" could be determined during this work, namely $\Delta E_{\text{Cis-Trans}}$, ${}^{Cis}\mu_4^B$, and ${}^{Cis}\mu_5^B$. During the calculation, however, the ${}^{\text{Trans}}\mu_0^B$ and ${}^{\text{Cis}}\mu_0^B$ B-type components of the permanent dipole moment for Trans-HONO and Cis-HONO, respectively, were maintained fixed at their values (see Eqs. (16) and (17)) obtained by Stark measurements [25]. The values obtained for the expansion of the far infrared transition moment operators and for $\Delta E_{\text{Cis-Trans}}$ are collected in **Table 3** together with their estimated uncertainties.

The results of this calculation is provided in the Supplementary Data of this paper, while **Table 4** provides a brief description of the results, in term of statistics, of the least squares fit computation.

V. Generation of the list of line positions, line intensities, and line shape parameters for the pure rotational bands of Trans-HONO and Cis-HONO conformers

5.1. *Computation of the total partition function*

Using the value $\Delta E_{Cis\text{-}Trans} = 95.8$ cm^{-1} and Eqs. (10) to (14), we have computed the total partition functions, $Z_{Tot}(T)$, in the T = 70 – 340 K temperature range. The results of that computation are provided as Supplementary data of the present article. These values differ from the values that we computed for the generation of the database for the ν_4 bands of Trans-HONO and Cis-HONO [12]. This was to be expected since, at that time, we used the $\Delta E_{Cis\text{-}Trans}$ = 143 cm^{-1} preliminary value for the computation of $Z_{Tot}(T)$. Clearly this (preliminary) line list at 11 µm will have to be revised by future investigations.

5.2. *Generation of a line list for the pure rotational bands of Trans- and Cis-HONO*

The method used to compute the line positions and line intensities was described earlier in the text. As far as the intensities are concerned, let us remind that these two bands are hybrid, with both A- and B-type components.

The lower state energy levels for both HONO conformers are defined relative to the position of the J = 0 level of the Trans-conformer. This means that the values

$$^{Trans}E_{Lower}(J, K_a, K_c) = {}^{Trans}E_{Rot}(J, K_a, K_c) \qquad \text{Eq. (24)}$$

$$\text{and} \quad {}^{Cis}E_{Lower}(J, K_a, K_c) = {}^{KM}E_{Cis\text{-}Trans} + {}^{Cis}E_{Rot}(J, K_a, K_c) \qquad \text{Eq. (25)}$$

are quoted for the Trans- and Cis-conformers, respectively. The quantities $^{Trans}E_{Rot}(J, K_a, K_c)$ and $^{Cis}E_{Rot}(J, K_a, K_c)$ are computed in a classical way using Dehayem's rotational constants. This list also includes the upper and lower state degeneracy, together with the Einstein coefficients [40], relevant for modelling astrophysical observations.

As far as line shape parameters are concerned, we adopted the same strategy than in Ref. [12]. The permanent dipole moments of Trans- and Cis-HONO have values, $^{Trans}\mu_0 = 1.930$ D and $^{Cis}\mu_0 = 1.428$ D, respectively [25]. Since these values are close to the water permanent dipole value ($\mu_0 = 1.855$ D [41]), it was decided to use for the HONO line shape parameters "a priori" values similar to those of water. More explicitly, the values:

$$\gamma_{Air} = 0.1 \text{ cm}^{-1}/\text{atm}, \ \gamma_{Self} = 0.4 \text{ cm}^{-1}/\text{atm}, \text{ and } n_{Air} = 0.7 \qquad \text{Eqs. (26)}$$

were implemented for the air-broadened half width, self-broadened half width and for the n-temperature dependent coefficient, respectively.

Table 5 provides a brief description of the line list, in terms of number of lines, frequency range and band intensities. In this line list, the accuracy of the line position is better than 0.001 cm^{-1} for most of the lines except for transitions that involve high quantum numbers ($J > 61$ or $K_a > 24$) that were not covered by the analysis of Dehayem et al. [24]. For the intensities, we estimate their accuracy at better than 8.5 %, and this error value accounts for the contribution of the line intensity measurements (about 6.5 %) and to the accuracy of the calculation (~ 2 %) taking into account the uncertainty on the $\Delta E_{Cis\text{-}Trans}$ energy difference.

VI. Discussion

6.1. *Comparison with the results of Sironneau et al.* [18]

During earlier work, the computation method differed from the present one. Indeed, in a preliminary step of that study [18], the (relative) intensities for Trans-HONO and Cis-HONO were fitted in two separate adjustment calculations, leading to the determination of the expansion of (relative) transition moment operators for Trans-HONO and Cis-HONO. Then, the zeroth order terms appearing in these expansions were scaled (in absolute) relative to ${}^{Trans}\mu_0^B$ and ${}^{Cis}\mu_0^B$ (see Eqs. (16-17)). Within this framework, three centrifugal distortion correcting terms were obtained, ${}^{Cis}\mu_4^B$, ${}^{Cis}\mu_4^B$, and ${}^{Trans}\mu_4^B$, associated to the expansion of the "absolute" B-type transition moment operators of the two conformers. At this point, we notice that, during their final line intensity computation for the Trans- and Cis- intensities, Sironneau *et al*. [18] used two <u>different</u> values of the partition functions (see Eq. (12):

$$ {}^{Trans}Z(T) = 8883 \text{ and } {}^{Cis}Z(T) = 8634 \qquad \text{Eq. (27)}$$

for Trans- and Cis-HONO respectively, while in the present work, the <u>total</u> partition function, ${}^{Tot}Z(T)$ (see Eq.(10)), was used for both conformers. Finally, in their final calculation [18], the relative concentrations, N_{Trans} and N_{Cis}, of Trans-HONO and Cis-HONO species were determined by comparing the observed ^{Trans}Abs'(296 K) and ^{Cis}Abs'(296 K), to the computed ${}^{Trans}k_{\tilde{\nu}}^N(T)$ and ${}^{Cis}k_{\tilde{\nu}}^N(T)$, and in this way the value of $\Delta E_{Cis\text{-}Trans}$ was determined using the expression:

$$\Delta E_{Cis\text{-}Trans} = -\,(kT/hc)\ln\left(\frac{N_{Cis}}{N_{Trans}}\right) \qquad \text{Eq.(28)}$$

Table 3 compares the intensity parameters obtained by Sironneau *et al*. [18] and in the present work.

It is clear that, for $\Delta E_{Cis\text{-}Trans}$, we obtained a value $\Delta E_{Cis\text{-}Trans} = 95.8 \pm 9.2$ cm^{-1} which is in excellent agreement with the results of Sironneau *et al*. ($\Delta E_{Cis\text{-}Trans} = 99 \pm 25$ cm^{-1}), but with an associated uncertainty which is significantly smaller. This is because the present calculation used a larger set of relative intensities and obtained at three different temperatures (240, 270 and 296 K).

For Cis-HONO, the values achieved for ${}^{Cis}\mu_4^B$ and for ${}^{Cis}\mu_6^B$ centrifugal distortion parameters are about ~1.5 times weaker than those obtained by Sironneau *et al*. [18]. On the other hand, the ${}^{Trans}\mu_4^B$ parameter could not be determined during our study. This is probably linked to the fact that a more accurate value was obtained during this work for the $\Delta E_{Cis\text{-}Trans}$ quantity. Indeed, Sironneau *et al*. [18] mentioned that during the least squares fit on the line intensities, the parameters for ${}^{Cis}\mu_k^B$ and for ${}^{Tans}\mu_l^B$ (k and l = 4 or 6) appeared to be highly correlated with $\Delta E_{Cis\text{-}Trans}$, and we confirm this fact.

6.2. *Other determination of $\Delta E_{Cis\text{-}Trans}$*

The detailed inter-comparison of literature values for $\Delta E_{Cis\text{-}Trans}$ was already presented by Sironneau *et al*. [18]. Among the various experimental determination of this parameter, only Varma and Curl [16] performed a resolved line intensity measurement at high resolution using microwave spectroscopy. In spite of a value 47% higher, the value that they obtained $\Delta E_{Cis\text{-}Trans} = 141 \pm 35$ cm^{-1} is not incompatible with the present results, as the error bars just barely overlap. The difference between Varna and Curl [16] and this work or Sironneau *et al*. [18] values is, probably due to the values they used for the B-type component operators that they used (${}^{Trans}\mu_0^B = 1.242$ and ${}^{Cis}\mu_0^B = 1.389$ D) which concern Trans-HO^{15}NO and Cis- HO^{15}NO [42], while Sironneau *et al*. [18] and the present work used the values (see Eqs. (16 - 17)) from Allegrini *et al*. [25] for the main HONO isotopic species.

6.3. *Comparison between the JPL line list* [5] *and the one generated in this work*

To our knowledge, the line list that is quoted at 300 K for the pure rotational bands of Trans-HONO and Cis-HONO in the JPL catalog [5] is the only one existing for HONO in this spectral region (from 21 to 9479568 MHz, i.e. from 0 to 316.2 cm^{-1}) in public access databases. This line list which is described in the "D047007.pdf", was used for the first detection of HONO in interstellar medium [4]. Indeed, twelve lines of HONO were identified towards component B of the low-mass protostellar binary IRAS 16293–2422 with the Atacama Large Millimeter/submillimeter Array (ALMA).

For an easier comparison with our line list, we use in the rest of the article a version of this JPL line list that we converted to a 296 K temperature.

In the present work, the positions were computed using the Dehayem' rotational parameters [24], and this means that the position differences with our list are mostly marginal. However, for Cis-HONO, we identify some weak discrepancies (up to 0.0005 cm^{-1}) for B-type transitions that involve high J and K_a rotational quantum numbers. When examining the FTS spectra recorded during this work in the 82-150 cm^{-1} region, these discrepancies corresponds also to mismatch between the observed and the JPL calculated line positions.

In this JPL list, the intensities were computed using the permanent dipole moment values from Stark measurements [25] (see Eqs. (16-17)). As in the present work, the Trans- and Cis- lower level energies and the total partition function $^{JPL}Z_{Tot}(T)$ were computed using the expressions quoted in Eqs. (24) and (25), and Eq. (10) respectively. However, these authors used for $\Delta E_{Cis\text{-}Trans}$ the value obtained by Varna and Curl [16]:

$$\Delta E_{Cis\text{-}Trans} = 141 \pm 35 \text{ cm}^{-1} \qquad \text{Eq . (29)}$$

differing from the value found in this work ($\Delta E_{Cis\text{-}Trans} = 95.8 \pm 9.2$ cm^{-1}).

As mentioned previously, $\Delta E_{Cis\text{-}Trans}$ contributes to the computation of the total partition function. **Table 6** compares the values for $^{JPL}Z_{Tot}(T)$ that are quoted at several temperatures (9.75 to 300 K) in the "D047007.pdf" JPL document with the values that we calculated during this work. Finally, for B-type transitions of Cis-HONO, another source of difference takes its origin in the expansion of the transition moment operator, that involves the non-zero values for the μ_4^B and μ_6^B centrifugal terms that are considered in our calculation, but ignored for the JPL list. When considering all these points the intensities in the two lists should differ of $\pm$ 20 to $\pm$ 40 %, depending on the A- or B-type of the transitions and of considered Trans- or Cis-HONO conformer.

However, more importantly, we also noticed that the B-lines involving low K_a values ($K_a = 0$, 1 and 2) in the upper or lower level of the transition are largely overestimated for both conformers in the JPL line list. Among these ones, the strongest mismatches occur for transitions involving $K_a = 1$ in the upper or lower levels. **Table 7** provides examples for errors for this type of transitions. The first three lines (at 333.92, 348.26 and 358.98 GHz) are those which "surprisingly enough" could not be observed towards the protostar IRAS 16293 B by the Atacama Large Millimeter/submillimeter Array instrument [4]. However, in our calculations, these transitions are predicted about five times weaker than in the list that was used in Ref. [4].

Table 7 also provides additional examples of transitions of the same type that are predicted by the JPL list in the 80.1 to 97.5 cm^{-1} spectral region with overestimated intensities compared to those observed in our FTS spectra. **Figs. 6, 7** and **8** show that these lines are (as expected by our computations) not detectable in our spectrum.

Because the calculation that we made and the parameters that we used for that computation are more accurate than the previous ones, our line list should be quite useful for future detections of HONO in astrophysical objects.

VII. Impact of the new line list on astrophysical detection of HONO

As already mentioned, the JPL line list was used for the first detection of HONO in interstellar medium [4]. It seems, however, that this astrophysical detection of HONO was not fully satisfactory since several lines of HONO, that are predicted to be strong enough to be observed, could not be detected in the target interstellar medium. Indeed, three undetected transitions of HONO at 333.925, 348.265 and 358.979 GHz were difficult to model satisfactorily (see Fig. 1 of the Ref. [4]). It was necessary to use a low excitation temperature (T_{ex}) of 100 K to not overproduce their fluxes significantly (above 3σ). With this new line list, we show that the models of the HONO transitions covered in the PILS large spectral survey are improved both for a T_{ex} of 100 K and 300 K (see **Figs. 9** and **10**). The fluxes of the three undetected transitions are not overproduced anymore and the flux of the transition at 362.398 GHz is now slightly lower. The χ^2 analysis gives now a best-fit model for a column density N = 1.9×10^{15} cm^{-2} and T_{ex} = 300 K, but the excitation temperature remains unconstrained. With a fixed T_{ex} = 100 K, the model is in good agreement with the observations as well. The column density is found to be 1×10^{15} cm^{-2} in this case. The column densities do not differ significantly from the ones published in [4] and the conclusions are not affected. However, it is certain that this new line list will make the identification of HONO in other astrophysical sources more robust.

CONCLUSION

High resolution spectra were recorded for nitrous acid present in an absorption cell in chemical equilibrium in mixtures of NO_2, NO and H_2O. These spectra were recorded at three different temperatures, 240, 270 and 296 K in the 50-200 cm^{-1} spectral region using the Bruker IFS125HR Fourier transform spectrometer on the AILES Beamline at Synchrotron SOLEIL. The line intensities for the B-type transitions of pure rotational bands of the Trans-HONO and Cis-HONO conformers were measured and introduced in least squares fit calculation for a new determination of the energy difference ($\Delta E_{Cis\text{-}Trans}$) between the ground vibrational states of the Cis- and Trans-HONO conformers of nitrous acid. In this way, we could significantly improve the accuracy on the energy difference : $\Delta E_{Cis\text{-}Trans} = 95.8 \pm 9.2$ cm^{-1} compared to ${}^{SIR}\Delta E_{Cis\text{-}Trans} = 99 \pm 25$ cm^{-1} in the previous study of Sironneau *et al*. [18]. During the same fit the centrifugal expansion terms involved in the transition moment operators of the B-type components of the pure rotation band of Cis-HONO were obtained. These data were used to compute the pure rotational bands of Trans-HONO and Cis-HONO that involves both the A- and B-type transitions of the rotation transitions for both Trans-HONO and Cis-HONO. This new line list is shown to be more accurate than the JPL line list for the same species, and of potential use for future detection of HONO, using new ALMA observations in Astrophysical objects.

SUPPLEMENTARY DATA

Three lists are provided as supplementary data

- The final line intensity computation (least squares fit computation).
- The partition function for HONO at various temperature
- The line list for HONO as described in Table 5 (in “HITRAN” type format [32]).

ACKNOWLEDGEMENTS

This work was supported by the French National program ANR (ANR-19-CE29-0013) through the « QUASARS » project. Soleil Support (project 20220356) is also acknowledged.

This paper makes use of the ALMA data ADS/JAO. ALMA#2013.1.00278.S. ALMA is a partnership of ESO (representing its member states), NSF (USA) and NINS (Japan), together

with NRC (Canada) and NSC and ASIAA (Taiwan), in cooperation with the Republic of Chile. The Joint ALMA Observatory is operated by ESO, AUI/NRAO, and NAOJ. AC received financial support from the European Research Council (ERC) under the European Union's Horizon 2020 research and innovation programme (ERC Starting Grant "Chemtrip", grant agreement No 949278).

REFERENCES

[1] Platt U, Perner D, Harris GW, Winer AM, Pitts Jr JN. Observations of nitrous acid in an urban atmosphere by differential optical absorption. Nature 1980;285:312–314.

[2] Yokelson RJ, Crounse JD, DeCarlo PF, Karl T, Urbanski S, Atlas E, Campos T, Shinozuka Y, Kapustin V, Clarke AD, Weinheimer A, Knapp DJ, Montzka DD, Holloway J, Weibring P, Flocke F, Zheng W, Toohey D, Wennberg PO, Wiedinmyer C, Mauldin L, Fried A, Richter D, Walega J, Jimenez JL, Adachi K, Buseck PR, Hall SR, Shetter R. Emissions from biomass burning in the Yucatan. Atmos Chem Phys 2009;9:5785–5812.

[3] Stockwell CE, Yokelson RJ, Kreidenweis SM, Robinson AL, DeMott PJ, Sullivan RC, Reardon J, Ryan KC, Griffith DWT, Stevens L. Trace gas emissions from combustion of peat, crop residue, domestic biofuels, grasses, and other fuels: configuration and Fourier transform infrared (FTIR) component of the fourth Fire Lab at Missoula Experiment (FLAME-4). Atmos Chem Phys 2014;14: 9727–9754.

[4] Coutens A, Ligterink NFW, Loison JC, Wakelam V, Calcutt H, Drozdovskaya MN, Jørgensen JK, Müller HSP, Van Dishoeck EF, Wampfler SF. The ALMA-PILS survey: First detection of nitrous acid (HONO) in the interstellar medium. Astronomy & Astrophysics 2019;623:L13.

[5] Pickett HM, Poynter RL, Cohen EA, Delitsky ML, Pearson JC, Müller SP. Submillimeter, millimeter, and microwave spectral line catalog. J Quant Spectrosc Radiat Transfer 1998;60:883–890.

[6] Clerbaux C, Boynard A, Clarisse L, George M, Hadji-Lazaro J, Herbin H, Hurtmans D, Pommier M, Razavi A, Turquety S, Wespes C, Coheur PF. Monitoring of atmospheric composition using the thermal infrared IASI/MetOp sounder. Atmos Chem Phys 2009;9:6041–6054.

[7] Clarisse L, R'Honi Y, Coheur PF, Hurtmans D, Clerbaux C. Thermal infrared nadir observations of 24 atmospheric gases. Geophys Res Lett 2011;38:L10802.

[8] Dufour G, Eremenko M, Siour G, Sellitto P, Cuesta J, Perrin A, Beekmann M. 24 h Evolution of an exceptional HONO plume emitted by the record-breaking 2019/2020 Australian wildfire tracked from space. Atmosphere 2022;13:1485.

[9] Whitburn S, Franco B, Bauduin S, Clerbaux C, *et al*. Identification of short and long-lived atmospheric trace gases from IASI space observations. Geophys Res Lett 2020;48: L091742.

[10] Guilmot JM, Godefroid M, Herman M. Rovibrational parameters for Trans-Nitrous acid. J Mol Spectrosc 1993;160;387-400.

[11] De Longueville H, Clarisse L, Whitburn S, Franco B, Bauduin S, Clerbaux C, Camy-Peyret C, Coheur PF. Identification of short and long-lived atmospheric trace gases from IASI space observations. Geophys Res Lett 2021;48:L091742.

[12] Armante R, Perrin A, Kwabia Tchana F, Manceron L. The ν_4 bands at 11 μm: linelists for the Trans- and Cis- conformer forms of nitrous acid (HONO) in the 2019 version of the GEISA database. Mol Phys 2021;e1951860:1–13.

[13] Kagann RH, Maki AG. Infrared Absorption Intensities of Nitrous Acid (HONO) Fundamental Bands. J Quant Spectrosc Radiat Transfer 1983;30:37-44.

[14] Jones LH, Badger RM, Moore GE. The infrared spectrum and the structure of gaseous nitrous acid. J Phys Chem 1951;19:1599–1604.

[15] McGraw GE, Bernitt DL, Hisatsune IC. Infrared spectra of isotopic nitrous acids. J Phys Chem 1966;45:1392–1399.

[16] Varma R, Curl RF. Study of the Dinitrogen Trioxide-Water-Nitrous Acid Equilibrium by Intensity Measurements in Microwave Spectroscopy. J Phys Chem 1976;80:402–409.

[17] Bongartz A, Kames J, Welter F, Schurath U. Near-UV absorption cross sections and trans/cis equilibrium of nitrous acid. J Phys Chem 1991;95:1076–1082.

[18] Sironneau V, Flaud JM, Orphal J, Kleiner I, Chelin P. Absolute line intensities of HONO and DONO in the far-infrared and re-determination of the energy difference between the trans- and cis-species of nitrous acid. J Mol Spectrosc 2010;259:100–104.

[19] Jursic BS. Density functional theory exploring the HONO potential energy surface. Chem Phys Lett 1999;299:334–344.

[20] Luckhaus D. Multi-arrangement quantum dynamics in 6D: cis–trans isomerization and 1,3-hydrogen transfer in HONO. Chem Phys 2004;304:79–90.

[21] Guo Y, Thompson DL. On combining molecular dynamics and stochastic dynamics simulations to compute reaction rates in liquids. J Phys Chem 2004;120:898–902.

[22] Luckhaus D. The vibrational spectrum of HONO: Fully coupled 6D direct dynamics. J Phys Chem 2003;118:8797–8806.

[23] Richter F, Hochlaf M, Rosmus P, Gatti F, Meyer HD. A study of the mode-selective trans–cis isomerization in HONO using ab initio methodology. J Phys Chem 2004;120:1306–1317.

[24] Dehayem-Kamadjeu A, Pirali O, Orphal J, Kleiner I, Flaud PM. The far-Infrared rotational spectrum of nitrous acid (HONO) and its deuterated species (DONO) studied by high-resolution Fourier transform spectroscopy. J Mol Spectrosc 2005;234:182–189.

[25] Allegrini M, Johns JWC, McKellar ARW, Pinson P. Stark spectroscopy with the CO Laser: the ν_2 fundamental bands of trans-and cis-nitrous acid, HNO_2, in the 6 μm region. J Mol Spectrosc 1980;79:446-454

[26] Brubach J-B, Manceron L, Rouzières M, Pirali O, Balcon D, Kwabia Tchana F, et al. Performance of the AILES THz-infrared beamline at SOLEIL for high resolution spectroscopy. AIP Conf Proc 2010;1214:81-4.

[27] Syomin DA, Finlayson-Pitts B. HONO decomposition on borosilicate glass surfaces: implications for environmental chamber studies and field experiments. Phys Chem Chem Phys 2003;5:5236–5242.

[28] Reymond-Laruinaz S, Faye M, Boudon V, Doizi D, Manceron L. High-resolution infrared spectroscopy and analysis of the v_2/v_4 bending dyad of ruthenium tetroxide. J Mol Spectrosc 2017;336:29-35.

[29] Roy P, Brubach J-B, Calvani P, de Marzi G, Filabozzi A, Gerschel A, et al. Infrared synchrotron radiation: from the production to the spectroscopic and microscopic applications. Nucl Instrum Methods Phys Res A 2001;467/468:426- 36.

[30] To be published.

[31] Faye M, Bordessoule M, Kanouté B, Brubach JB, Roy P. Manceron L. Improved mid infrared detector for high spectral or spatial resolution and synchrotron radiation use. Rev. Sci. Inst. 2016;87:063119.

[32] Gordon IE, Rothman LS, Hargreaves RJ, Hashemi R, Karlovets EV, Skinner FM, Conway EK, Hill C, Kochanov RV, Tan Y, Wcisło P, Finenko AA, Nelson K, Bernath PF, Birk M, Boudon V, Campargue A, Chance KV, Coustenis A, Drouin BJ, Flaud J-M, Gamache RR, Hodges JT, Jacquemart D, Mlawer EJ, Nikitin AV, Perevalov VI, Rotger M, Tennyson J, Toon GC, Tran H, Tyuterev VG, Adkins EM, Baker A, Barbe A, Canè E, Császár AG, Dudaryonok A, Egorov O, Fleisher AJ, Fleurbaey H, Foltynowicz A, Furtenbacher T, Harrison JJ, Hart-mann J-M, Horneman V-M, Huang X, Karman T, Karns J, Kassi S, Kleiner I, Kof-man V, Kwabia–Tchana F, Lavrentieva NN, Lee TJ, Long DA, Lukashevskaya AA, Lyulin OM, Makhnev VY, Matt W, Massie ST, Melosso M, Mikhailenko SN, Mondelain D, Müller HSP, Naumenko OV, Perrin A, Polyansky OL, Raddaoui E, Raston PL, Reed ZD, Rey M, Richard C, Tóbiás R, Sadiek I, Schwenke DW, Starikova E, Sung K, Tamassia F, Tashkun SA, Vander Auwera J, Vasilenko IA, Vigasin AA, Villanueva GL, Vispoel B, Wagner G, Yachmenev A, Yurchenko SN. The HITRAN2020 molecular spectroscopic database. J Quant Spectrosc Radiat Transf 2022;277:107949.

[33] Tudorie M, Foldes T, Vandaele AC, Vander Auwera J. CO_2 Pressure broadening and shift coefficients for the 1-0 band of HCl and DCl. J Quant Spectrosc Radiat Transf 2012;113:1092–101.

[34] Daneshvar L, Foldes T, Buldyreva J, Vander Auwera J. Infrared absorption by pure CO_2 near 3340 cm^{-1}: measurements and analysis of collisional coefficients and line-mixing effects at subatmospheric pressures. J Quant Spectrosc Radiat Transf 2014;149:258–74.

[35] Wells R. Rapid approximation to the Voigt/Faddeeva function and its derivatives. J Quant Spectrosc Radiat Transf 1999;62:29–48.

[36] Ballard J, Knight RJ, Vander Auwera J, Herman M, Di Lonardo G, Masciarelli G, Nicolaisen FM, Beukes JA, Christensen LK, McPheat R, Duxbury G, Freckleton R, Shine KP. An intercomparison of laboratory measurements of absorption cross-sections and integrated absorption intensities for HCFC-22. J Quant Spectrosc Radiat Transf 2000;66:109-28.

[37] Fischer J, Gamache RR, Goldman A, Rothman LS, Perrin A. Total internal partition sums in the 2000 edition of the HITRAN database. J Quant Spectrosc Radiat Transfer 2003;82:401–412.

[38] Guilmot JM, Mélen F, Herman M. Rotational parameters for Cis-HONO. J Mol Spectrosc 1993;160**:**401–410.

[39] Flaud JM, Camy-Peyret C, Toth RA. Water vapour line Parameters from microwave to medium Infrared (An atlas of $H_2{}^{16}O$, $H_2{}^{17}O$ and $H_2{}^{18}O$ line positions and Intensities between 0 and 4350 cm^{-1}). 1st ed. Oxford: Pergamon Press; 1981.

[40] Simeckova M, Jacquemart D, Rothman LS, Gamache RR, Goldman A. Einstein A-coefficients and statistical weights for molecular absorption transitions in the HITRAN database. J Quant Spectrosc Radiat Transf 2006;98:130–155.

[41] Shostak SL, Ebenstein WL, Muenter JS. The dipole moment of water. I. dipole moments and hyperfine properties of H_2O and HDO in the ground and excited vibrational states. J Phys Chem 1991;94:5875-5882.

[42] Cox AP, Brittain AH, Finnigan DJ. Microwave spectrum, structure, dipole moment and quadrupole coupling constants of cis and trans nitrous acids. Trans Faraday Soc 1971;67:2179.

List of Tables

Table 1.
Total pressures in the equilibrium mixtures, partial pressures of HONO (in hPa), temperature (in K), absorption path length (in m) and number of interferograms averaged to yield the corresponding spectrum (# scans). All the spectra were recorded at a resolution of 0.0014 cm^{-1} (equal to 0.9 divided by the maximum optical path difference) and an entrance aperture diameter of the interferometer equal to 2.5 mm. The uncertainty on the partial pressure of HONO was estimated to 2% of the value given.

#	Total pressure in the mixture (hPa)	P_{HONO} (hPa)	T (K)	Optical path length (m)	# Scans
S1	1.4509	0.0120 (2)	296 ± 1	10.96 (3)	644
S2	2.9961	0.0252 (5)	296 ± 1	19.12 (6)	728
S3	2.5102	0.0461 (9)	270 ± 1	19.12 (6)	504
S4	1.5744	0.0397 (8)	240 ± 1	19.12 (6)	308
S5	2.9575	0.0265 (5)	296 ± 1	10.96 (3)	616

Table 2.

Number of lines measured and included in the intensity fits; spectral range and lower state J and K_a values.

	J range	K_a range	Spectral range (cm^{-1})	T (K)	Number of lines
trans-HONO	16–54	9–22	85–129	240 270 296	126 133 129
	8–43	5–20	46–121.1	296[a]	120[a]
cis-HONO	16–57	10–20	82.6–115.6	240 270 296	61 60 64
	9–41	6–22	43.2–118.6	296[a]	94[a]

[a]From Sironneau *et al.* [18]

Table 3.

Transition dipole moment constants for the B-type pure rotation bands of Trans-HONO and Cis-HONO, and value of the $\Delta E_{Cis\text{-}Trans}$ energy difference.

		This work		Sironneau *et al*. [18]	
		Trans-HONO	Cis-HONO	Trans-HONO	Cis-HONO
φ_x	μ_0^B in D [b]	1.347[a]	1.394[a]	1.347[a]	1.394[a]
$\{i\varphi_y, J_z\}$	μ_4^B in D [b]	-	-3.72(86)×10^{-3}	-3.309(60)×10^{-3}	-5.56(95)×10^{-3}
$\{i\varphi_z, iJ_y\}$	μ_6^B in D [b]	-	1.09(40)×10^{-3}	-	1.67(45)×10^{-3}
Number of lines		508	279	120	94
$\Delta E_{Cis\text{-}Trans}$ (in cm^{-1})		95.8 ± 9.2		99 ± 25	

(a) Maintained fixed at the values from Allegrini *et al*. [25].

(b) Values in Debye, 1 D = 3.33564 × 10^{-30} C m.

Table 4.

Statistical analysis for the line intensity computation: combined least squares calculation for the four sets of experimental relative intensities.

Source	**240 K** this work	**270 K** this work	**296 K** this work	**296 K** Sironneau *et al*. [18]	**All**
Number of lines:	187	193	193	214	787
$0 \leq \delta < 8$ %	36.9 %	53.9 %	44.6 %	48.6 %	46.1%
$8 \% \leq \delta < 10$ %	12.3 %	6.7 %	8.8 %	9.3 %	9.3 %
$10 \% \leq \delta < 20$ %	34.8 %	23.3 %	31.1 %	24.8 %	28.3%
$20 \% \leq \delta < 40$ %	13.9 %	15.5 %	14.5 %	15.4 %	14.9 %
$40 \% \leq \delta < 50$ %	2.1 %	0.5 %	1.0 %	1.4 %	1.3 %
$50 \% \leq \delta < 60$ %				0.5 %	0.1 %

$\delta = (Int_{Obs}\text{-}Int_{Calc})/Int_{Obs}$ in %

Table 5.
Results of the present line intensity and position computation at 296 K.

Conformer	Type	Nb of lines	Band intensity(1)	σ_{Min} (2)	σ_{Max} (2)	Int_{Min} (1)	Int_{Max} (1)
Trans	A-type	5912	0.329×10^{-18}	0.003	75.81	0.35×10^{-29}	0.78×10^{-21}
	B-type	11442	0.138×10^{-17}	0.044	235.84	0.24×10^{-27}	0.21×10^{-20}
	total		*1.704×10^{-18}*				
Cis	A-type	2869	0.107×10^{-19}	0.141	75.87	0.15×10^{-27}	0.25×10^{-22}
	B-type	10948	0.757×10^{-18}	0.075	209.70	0.43×10^{-27}	0.12×10^{-20}
	total		*0.767×10^{-18}*				
Total		**31171**	**0.249×10^{-17}**				

(1) In $cm^{-2}/(molecule.cm^{-1})$ @ 296 K

(2) Frequency range in cm^{-1}

Table 6.

Examples of the Total partition function $Z^{Tot}(T)$ computed during this work and comparisons with the JPL catalog values [5]:

Temperature (K)	JPL (a)	This work (final value) (b)
9.375 K	43.5646	43.564
18.75 K	122.0725	122.145
37.50 K	346.0466	352.451
75.0 K	1050.7792	1125.80
150 K	3537.0834	3877.80
225 K	7553.7830	8229.18
300 K	11962.7876	14716.67

(a) JPL catalog values with $\Delta E_{Cis\text{-}Trans} = 141\ cm^{-1}$ [16].

(b) Present work with $\Delta E_{Cis\text{-}Trans} = 95.8 \pm 9.2\ cm^{-1}$.

Table 7.

Comparison between computed intensities at 296 K in this work and in the JPL catalog

HONO conformer	Assignment	Sigma GHz	Sigma cm^{-1}	JPL[$]	This work [$]	Ratio JPL/This work
Trans	21 1 20 - 21 0 21	333.9250	11.1385	0.486×10^{-21}	0.101×10^{-21}	4.8
Cis	20 1 19 - 20 0 20	348.2649	11.6169	0.366×10^{-21}	0.641×10^{-22}	5.7
Trans	22 1 21 - 22 0 22	358.9791	11.9743	0.549×10^{-21}	0.106×10^{-21}	5.2
Cis	42 3 39 - 41 2 40	2402.719	80.1460	0.369×10^{-21}	0.148×10^{-22}	27
Trans	45 3 42 - 44 2 43	2405.972	80.2545	0.445×10^{-21}	0.247×10^{-22}	18
Trans	47 2 45 - 46 1 46	2840.938	94.7635	0.658×10^{-21}	0.773×10^{-23}	85
Cis	45 2 43 - 44 1 44	2846.929	94.9633	0.457×10^{-21}	0.389×10^{-23}	115
Trans	48 2 46 - 47 1 47	2909.114	97.0376	0.578×10^{-21}	0.649×10^{-23}	89
Cis	46 2 44 - 45 1 45	2916.013	97.2677	0.402×10^{-21}	0.334×10^{-23}	120
Cis	35 4 31 - 34 1 34	2922.900	97.4975	0.344×10^{-21}	0.836×10^{-24}	411

[$] Line intensities in $cm^{-1}/(molecule.cm^{-2})$ at 296 K

List of Figures

Figure 1.
Portion of the spectra observed in this work at high spectral resolution (0.0014 cm^{-1}) using synchrotron radiation source with 500 mA ring current. Details of the experimental conditions are given in **Table 1**. The observed spectra are in transmittance and shifted vertically for clarity.

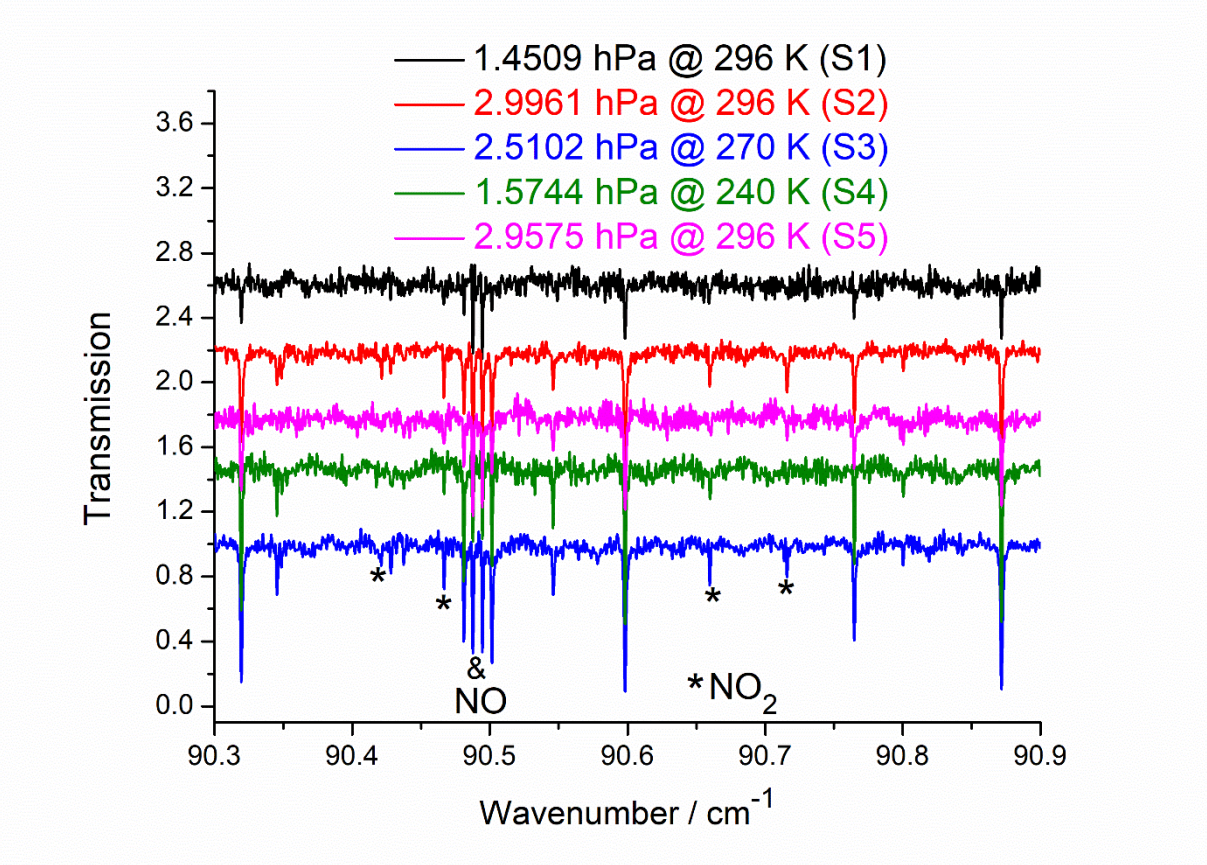

Figure 2.
Expanded region between 85 and 88 cm^{-1} observed in this work with synchrotron radiation, compared with that observed by using a classical Globar source and high total pressure of 20 hPa, by Sironneau *et al*. [18]. Transitions marked with symbols belong to the species: H_2O, NO_2 or NO. The new experimental conditions resulted in a fully resolved spectrum.

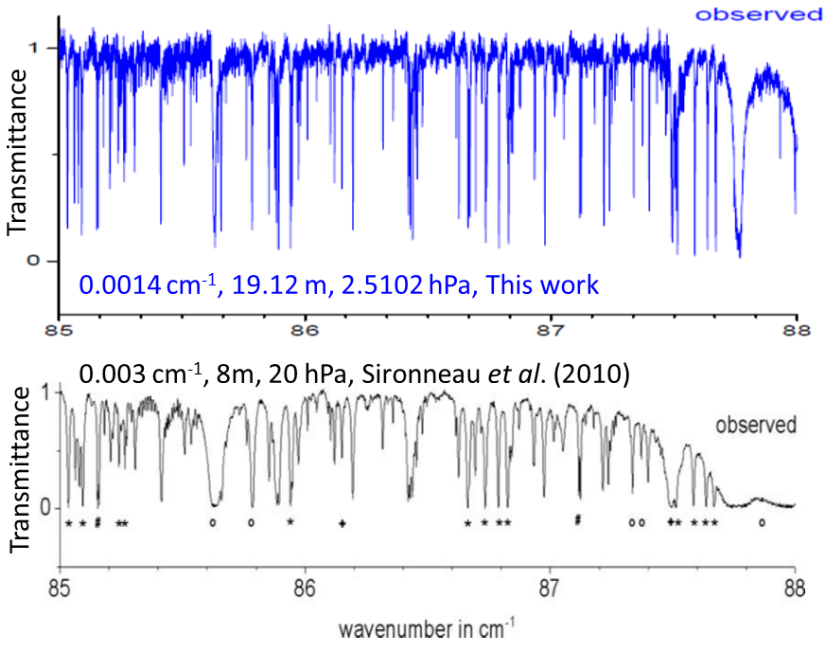

Figure 3.
The upper panel presents a small part of the spectrum of HONO lines (S3 in **Table 1**; open circles) overlaid by the corresponding best-fit calculated spectrum (solid line) obtained with a source aperture diameter of 2.5 mm, a maximum optical path difference of 642.857 cm and a Voigt profile. The lower panel shows the percent differences between the observed and calculated spectra.

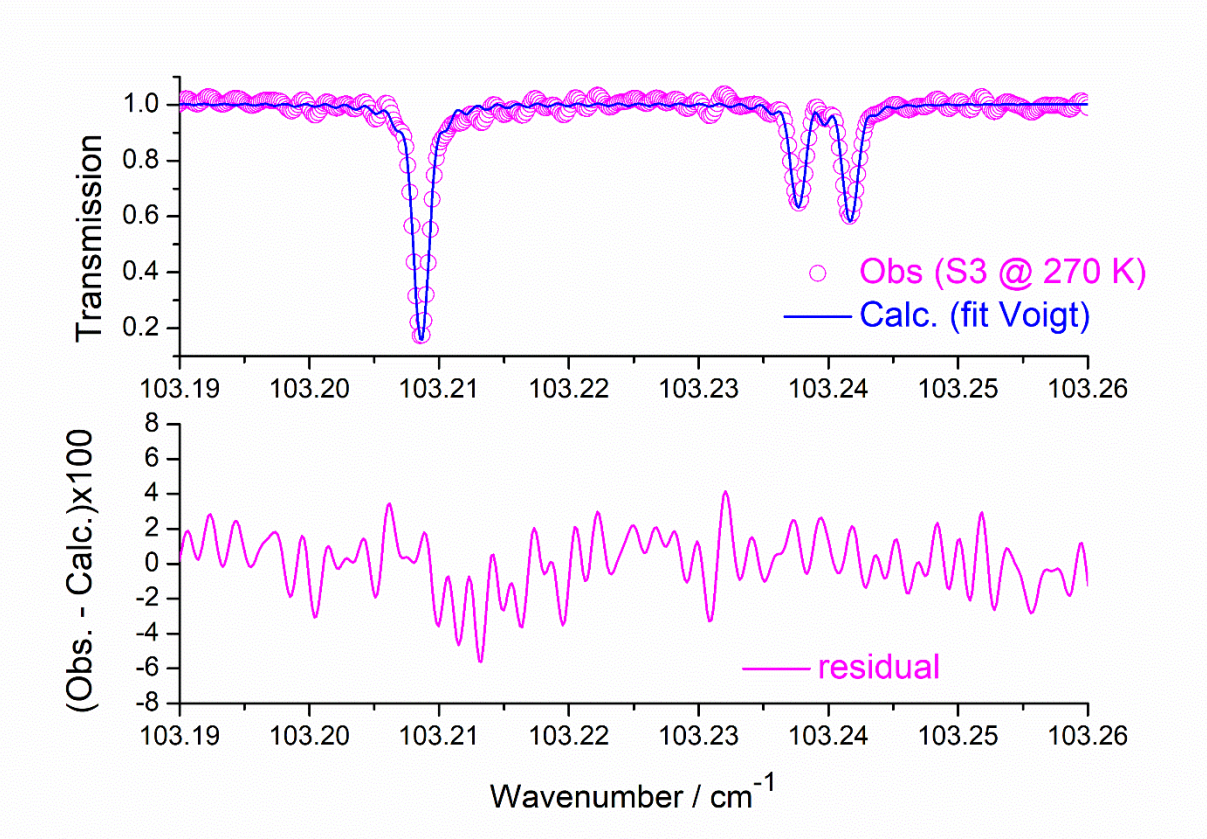

Figure 4.
Results of the mono-spectrum analysis applied to spectra S2, S3 and S4 at 296, 270 and 240 K, respectively. The top panel shows the observed spectra and the lower panel presents the best-fit residuals corresponding to spectra S2, S3 and S4.

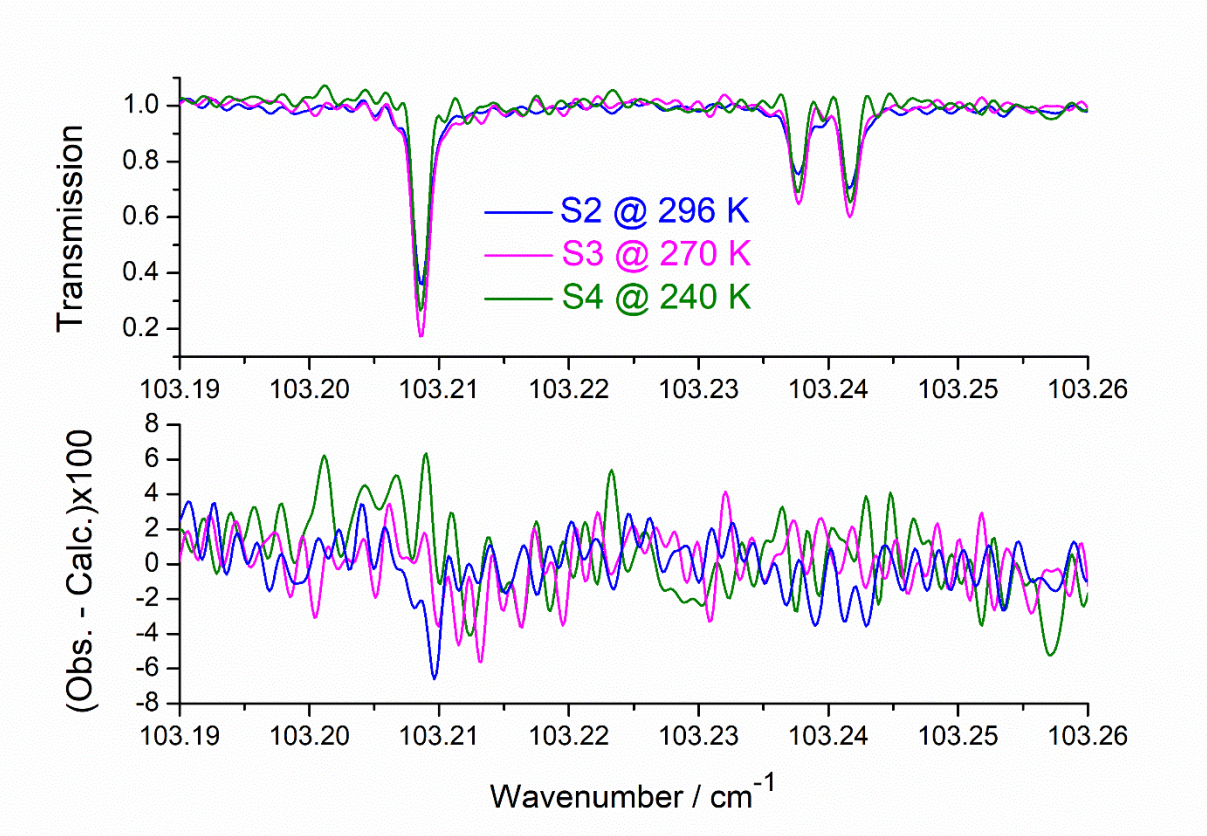

Figure 5.
Comparison between various sources of relative uncertainty on the measured intensities of 3 selected lines of high, medium and low intensity: ^{R}Q (19,16), ^{R}Q (32,14) and ^{R}Q (30,16).

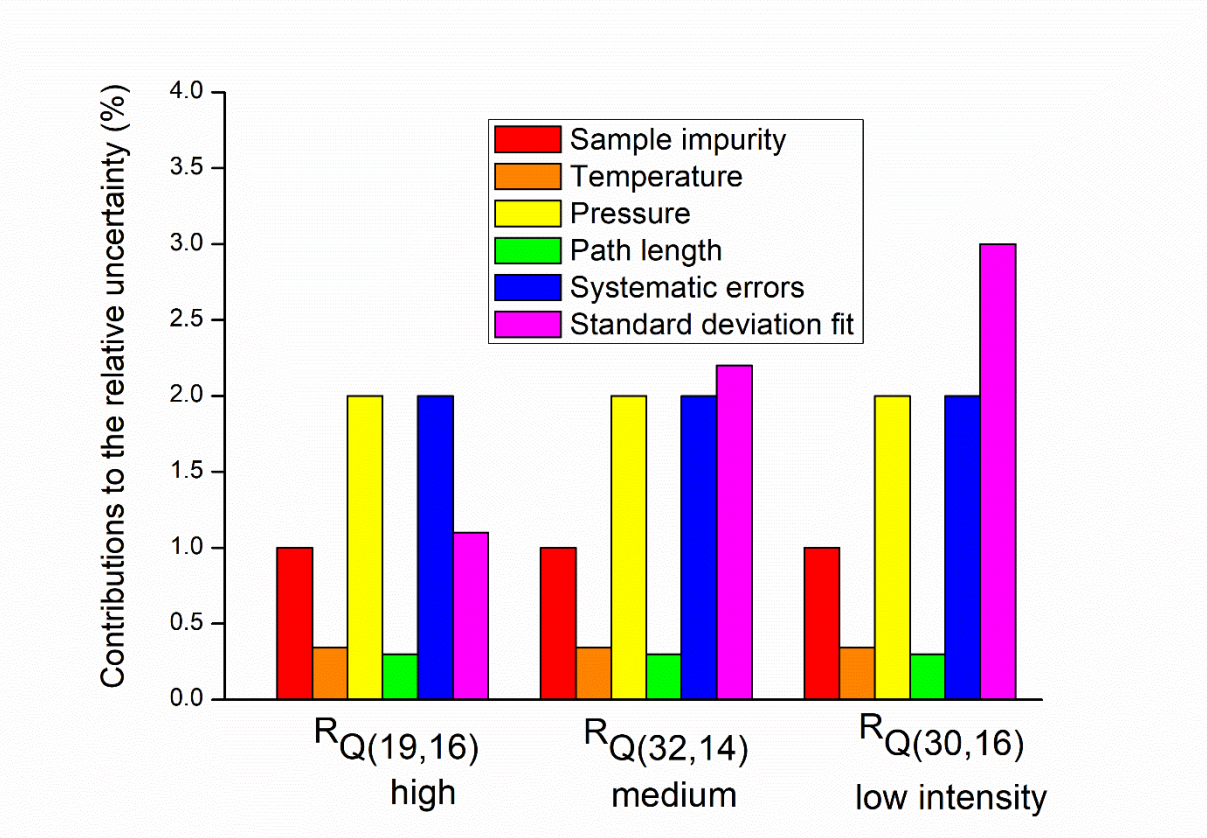

Figure 6.

Portion of the spectrum S2 recorded during this work near 80.2 cm^{-1}. The experimental conditions are given in **Table 1**. We compare the experimental spectrum to computed spectra generated using our line list and the JPL catalog. It is clear that several lines which are listed in **Table 7** and which are indicated here by stars, have overestimated intensities in the JPL line list. Impurities due to H_2O and NO_2 are identified on the spectrum.

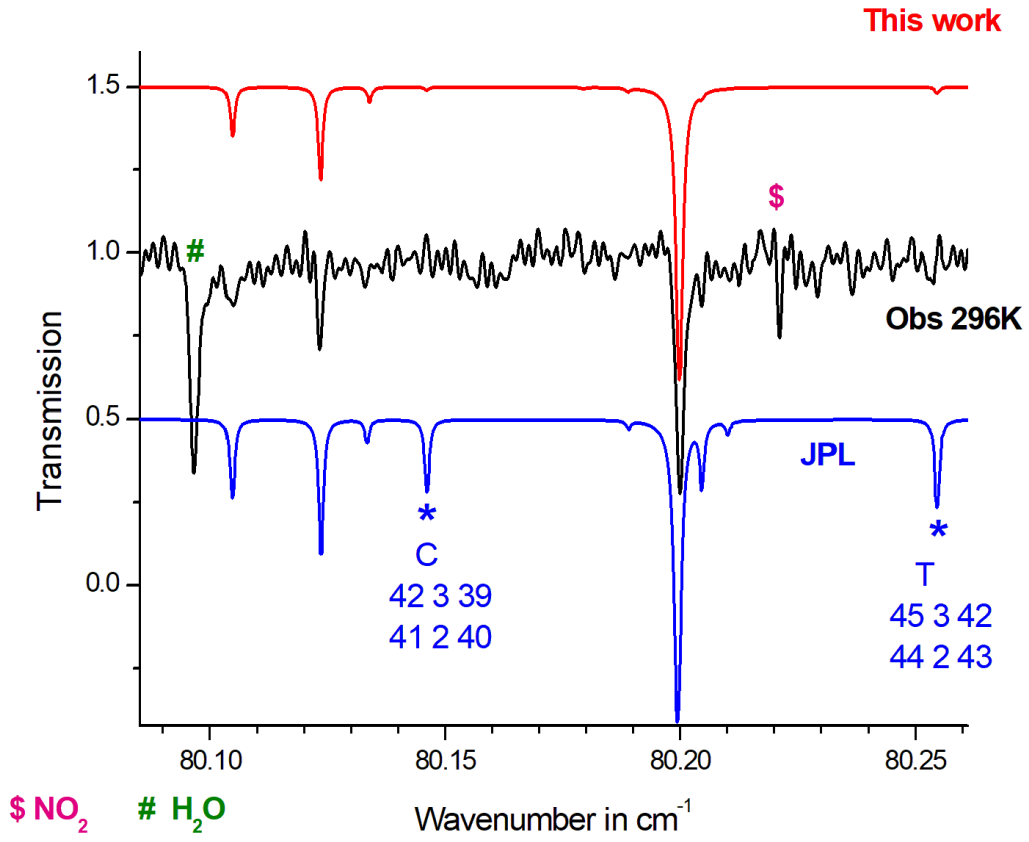

Figure 7.

Portion of the spectrum S2 recorded during this work near 94.85 cm^{-1}. The experimental conditions are given in **Table 1**. We compare the experimental spectrum to computed spectra generated using our line list and the JPL catalog. It is clear that several lines which are listed in **Table 7** and which are indicated here by stars, have overestimated intensities in the JPL line list. Impurities due to H_2O and NO_2 are identified on the spectrum.

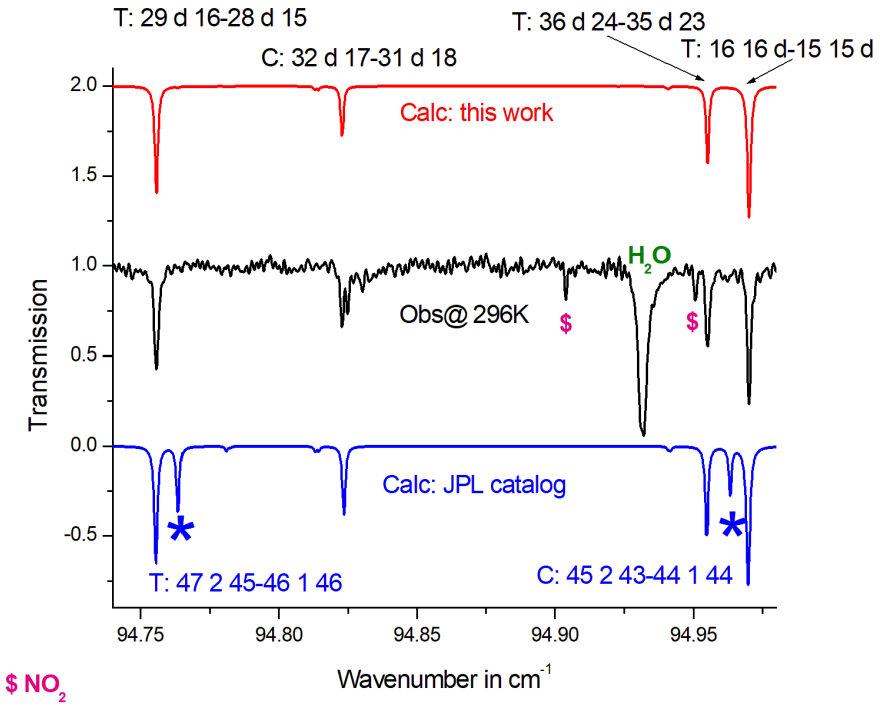

Figure 8.

Portion of the spectrum S2 recorded during this work near 97.3 cm^{-1}. The experimental conditions are given in **Table 1**. We compare the experimental spectrum to computed spectra generated using our line list and the JPL catalog. It is clear that several lines which are listed in **Table 7** and which are indicated here by stars, have overestimated intensities in the JPL line list. Impurities due to H_2O and NO_2 are identified on the spectrum.

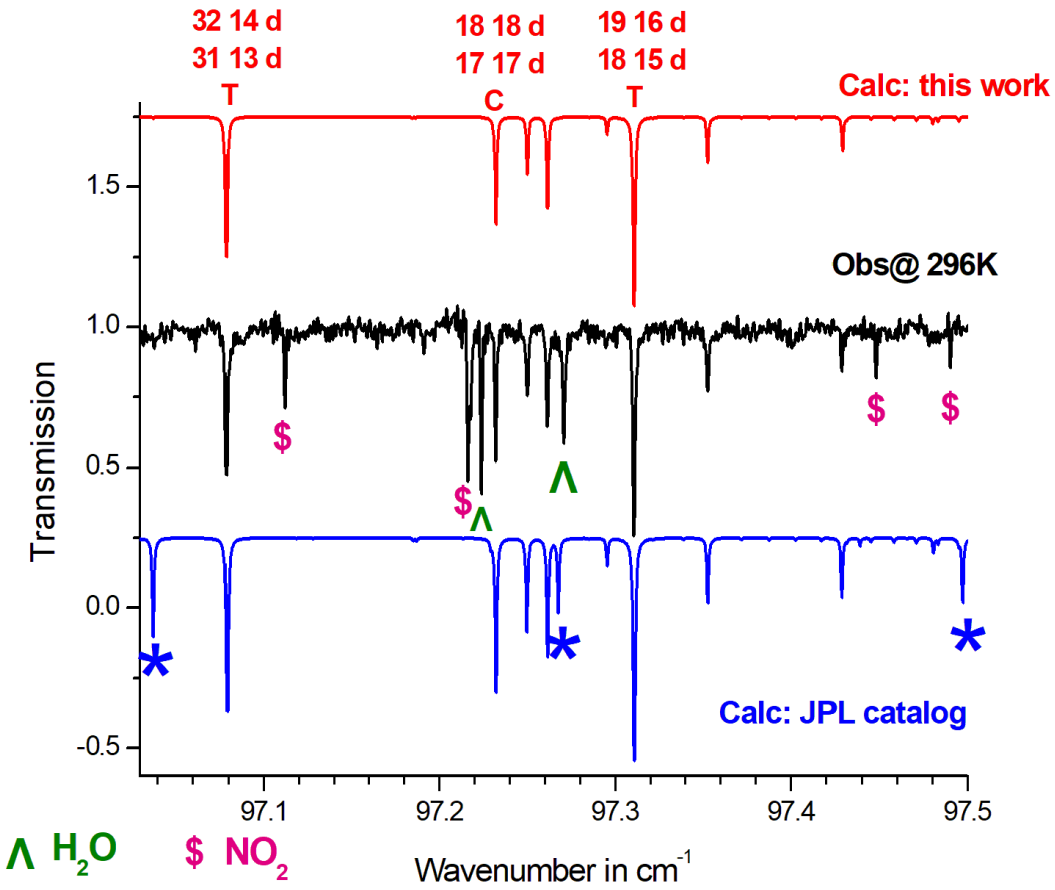

Figure 9.

Comparison of the ALMA observations of the HONO transitions towards the protostar IRAS16293 B (black) with the model obtained with the JPL line list for T_{ex} = 100 K and $N = 9\ 10^{14}$ cm^{-2} ([4], blue dashed line) and the one obtained with our new line list for similar parameters (red solid line).

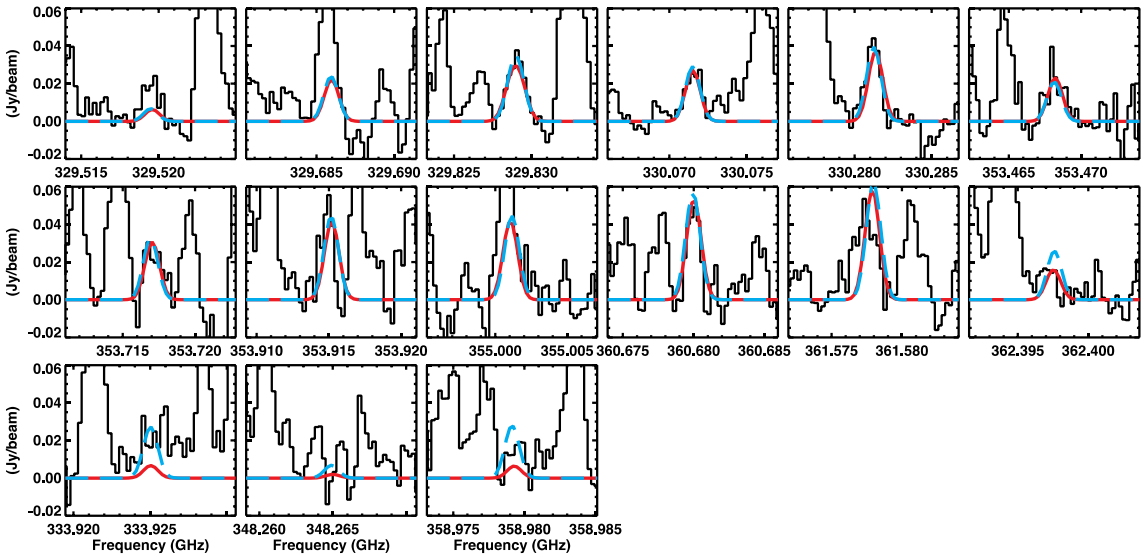

Figure 10.

Comparison of the ALMA observations of the HONO transitions towards the protostar IRAS16293 B (black) with the model obtained with the JPL line list for T_{ex} = 300 K and N = 1.4 10^{15} cm^{-2} ([4], blue dashed line) and the one obtained with our new line list for similar parameters (red solid line).